Materials Today Communications 52 (2026) 115054

Contents lists available at ScienceDirect

Materials Today Communications

journal homepage: www.elsevier.com/locate/mtcomm

Interphase-mediated toughening of poly-(lactic acid) by hierarchical carbon nanotube and carbon fiber reinforcement

Roland Petrény [a,*], László Almásy [b], László Mészáros [a,c]

[a] Department of Polymer Engineering, Faculty of Mechanical Engineering, Budapest University of Technology and Economics, Műegyetem rkp. 3, Budapest H-1111, Hungary
[b] Institute for Energy Security and Environmental Safety, HUN-REN Centre for Energy Research, Konkoly Thege Miklós út 29-33, Budapest H-1121, Hungary
[c] HUN-REN-BME Research Group for Composite Science and Technology, Műegyetem rkp. 3, Budapest H-1111, Hungary

ARTICLE INFO

Keywords:
Polylactic acid
Carbon nanotubes
Carbon fibers
Interphase structure
Toughening

ABSTRACT

Polylactic acid composites reinforced with carbon nanotubes (CNTs) and carbon fibers (CFs) were investigated to assess their morphological and mechanical properties. Nanocomposites (0–1 wt% CNT) and hybrid composites (30 wt% CF with 0–1 wt% CNT) were analyzed using small-angle neutron scattering, X-ray diffraction, differential scanning calorimetry, and mechanical testing. The CNT-only composites showed CNT aggregation, while hybrid composites exhibited improved CNT dispersion and extended structures due to CF-assisted distribution. Both reinforcements increased the rigid amorphous phase and reduced crystallinity, suggesting refined crystalline structures. X-ray diffraction revealed enhanced lateral crystallite growth, particularly in CF-containing systems, indicating the crystal nucleating behavior of the reinforcing materials. Mechanical testing demonstrated significant improvements in tensile strength, elongation at break, and toughness in hybrid composites, with optimal performance at 0.25–1 wt% CNT. These results highlight a synergistic effect between CNTs and CFs, enhancing both dispersion and composite performance.

1. Introduction

Polylactic acid (PLA) has emerged as one of the most widely adopted bioplastics in recent years due to its renewable origin, biodegradability, and favorable processability. Derived from agricultural feedstocks such as corn starch or sugarcane, PLA offers a promising alternative to petroleum-based plastics in the context of growing environmental concerns and increasing emphasis on sustainable material development [1–3]. Its biobased origin allows for the release of biogenic carbon dioxide upon combustion, contributing to a more carbon-neutral lifecycle when compared to conventional fossil-derived polymers [3].

Despite these advantages, PLA exhibits certain limitations that restrict its applicability in high-performance or technical applications. Most notably, its inherent brittleness and relatively low impact resistance present challenges for use as a structural material. To address these issues, various reinforcement strategies have been explored, including the incorporation of natural fibers such as flax or jute. These natural reinforcements not only align with PLA's biodegradability and sustainability profile but also offer improvements in mechanical strength [4,5]. However, the extent of such enhancements is limited, and natural fibers tend to increase PLA's sensitivity to moisture, which can compromise dimensional stability and long-term performance [6,7].

To overcome the limitations associated with natural reinforcements, synthetic fibers such as carbon fibers have been investigated as alternatives. While the incorporation of carbon fibers compromises the biodegradability of the composite, it significantly enhances the mechanical performance, enabling PLA-based materials to be used in more demanding engineering applications [8–11]. Importantly, the biogenic origin of PLA means that even when combined with non-biodegradable reinforcements, the composite retains a lower environmental footprint than fully petroleum-based materials, particularly in terms of greenhouse gas emissions over its lifecycle [12,13].

In parallel with fiber reinforcement, the addition of nanoparticles—especially carbon nanotubes (CNTs)—has gained attention as a means of improving the toughness and functional properties of PLA. CNTs are known for their exceptional mechanical, electrical, and thermal properties, and when effectively dispersed within a polymer matrix, they can facilitate stress transfer, homogenize stress distribution, and increase tensile strength and modulus [14–18]. Moreover, the inclusion of CNTs can impart multifunctional properties, such as electrical and

* Corresponding author.
E-mail address: petrenyr@pt.bme.hu (R. Petrény).

https://doi.org/10.1016/j.mtcomm.2026.115054
Received 4 December 2025; Received in revised form 22 February 2026; Accepted 23 March 2026
Available online 23 March 2026
2352-4928/© 2026 The Author(s). Published by Elsevier Ltd. This is an open access article under the CC BY-NC license (http://creativecommons.org/licenses/by-nc/4.0/).

thermal conductivity, broadening the range of potential applications for PLA-based materials [19–22].

Nevertheless, the benefits of nanoparticle reinforcement are highly dependent on factors such as dispersion quality, interfacial interactions, and their effect on the crystallization process. CNTs exhibit strong interparticle interactions, leading to aggregation and making effective dispersion difficult. The aggregates can act as stress concentrators, thereby degrading the mechanical performance and potentially increasing brittleness. [23,24]. Moreover, reinforcement-induced changes in PLA crystallization kinetics can alter the crystalline morphology, thereby affecting the mechanical performance of the composite. [25]. Reinforcements that serve as nucleating agents can promote the formation of crystalline regions around the fibers or particles, facilitating a more gradual stress transfer across the fiber–matrix interface. This crystalline interphase may contribute to improved toughness and higher failure loads [26–28]. In contrast, if the additives hinder polymer chain mobility and suppress crystallization, a rigid amorphous phase may form around the inclusions, resulting in weaker interfacial adhesion and diminished mechanical properties compared to a crystalline interphase.

Given these complexities, the combined effects of different reinforcing agents—especially at the nano- and microscale—require further investigation to optimize composite formulations. In particular, the interaction between carbon nanotubes and carbon fibers within a PLA matrix presents an intriguing opportunity for a synergistic reinforcing effect, potentially yielding materials with superior strength, toughness, and multifunctionality. The present research aims to systematically explore the individual and combined effects of carbon nanotubes and carbon fibers on the microstructure and mechanical properties of PLA composites. By examining the influence of these reinforcements on crystallization behavior, phase morphology, and mechanical performance, this study seeks to deepen the understanding of structure–property relationships in PLA-based composites. Ultimately, the insights gained will support the rational design and optimization of high-performance materials with a reduced environmental footprint.

2. Materials and methods

2.1. Sample preparation

To examine the influence of carbon nanotubes (CNTs) on the morphology and mechanical properties of PLA composites, two series of materials were prepared: a nanocomposite series with varying CNT content (0, 0.25, 0.5, 0.75 and 1 wt%), and a hybrid composite series containing 30 wt% carbon fiber (CF), with CNT contents matched to those in the nanocomposite series (0, 0.25, 0.5, 0.75, and 1 wt%).

The matrix material was Ingeo 4043D PLA (NatureWorks LLC, USA), a semi-crystalline bioplastic with a tensile strength of 53 MPa, a tensile modulus of 3.6 GPa, elongation at break of 6%, a density of 1.24 g/cm^3 , and a melt flow index (MFI) of 6 g/10 min (2.16 kg/210 °C). Its 4.8% D-lactide content enables crystallization under appropriate processing conditions.

The nanoreinforcement used was Nanocyl NC7000 multi-walled carbon nanotubes (CNT, Nanocyl SA, Belgium), synthesized via catalytic chemical vapor deposition. These CNTs had an average diameter of 9.5 nm, an average length of 1.5 μm, a specific surface area of 250–300 m^2/g, and a carbon purity of 90 wt%, with less than 1 wt% transition metal oxides.

As microfiber reinforcement, PANEX PX35 chopped carbon fibers (Zoltek Zrt., Hungary) were used, featuring a tensile strength of 3800 MPa, a tensile modulus of 242 GPa, elongation at break of 1.5%, and a density of 1.81 g/cm^3 . The fibers, approximately 7.2 μm in diameter and initially 6 mm long, were supplied with a silane-based sizing designed for use with polar polymer matrices, making them suitable for PLA as well.

The manufacturing methodology, including compounding and injection molding procedures, follows the process described in our previous work [14]. Prior to compounding, PLA granules were dried at 80 °C for 4 h in a Faithful WGLL−125 BE drying oven (Huanghua Faithful Instrument Co., Ltd., China). The reinforcing materials (carbon fibers and/or carbon nanotubes) were mechanically premixed with the dried PLA, followed by melt compounding using a Labtech LTE 26–44 twin-screw extruder (Labtech Engineering Co., Ltd., Thailand) at a screw speed of 25 rpm. The barrel temperature profile ranged from 180 °C to 200 °C, with a die temperature of 190 °C. The extrudate was pelletized into ~4 mm granules using a Labtech LZ−120/VS granulator and subsequently redried under the same conditions before molding.

Tensile specimens (Type 1 A) were prepared in accordance with EN ISO 527–2:2019 using an Arburg Allrounder Advance 270S 400–170 injection molding machine (Arburg GmbH, Germany). Processing parameters included a melt temperature of 200 °C, mold temperature of 25 °C, and an injection pressure of 1200 bar. Since PLA crystallizes relatively slowly under typical processing conditions, the cooling rate inherent to injection molding was sufficient to prevent crystallization, resulting in an amorphous PLA matrix (APLA) [29]. To obtain semi-crystalline composites (PCPLA), the molded specimens were annealed at 100 °C for 1 h in a Faithful WGLL−125 BE oven, placed between press plates to minimize dimensional shrinkage [14].

For small-angle neutron scattering (SANS) and X-ray diffraction (XRD) analyses, rectangular specimens with dimensions of 20 mm × 20 mm and a thickness of 2 mm were machined from the gripping ends of injection-molded tensile bars using a Roland MDX−540 4-axis milling machine.

2.2. Characterization methods

SANS measurements were conducted on the Yellow Submarine instrument at the Budapest Neutron Centre [30,31]. The experiments were performed at room temperature with a mean neutron wavelength of 4.2 Å and sample-to-detector distances of 115 and 535 cm. Each measurement was carried out with an average counting time per sample of 3 h. The pair-distribution functions were fitted to the scattering data using the SasView 6 software.

Differential scanning calorimetry was carried out on a TA Instruments Q2000 differential scanning calorimeter (TA Instruments, Delaware, USA) under a nitrogen atmosphere (flow rate: 50 mL/min), using modulated DSC (MDSC) mode. The temperature range was 0–250 °C, with heating and cooling rates of 5 °C/min. The modulation amplitude was 1 °C with a period of 60 s. Sample masses ranged from 10 to 15 mg. For each material, three measurements were conducted and the results averaged. Crystallinity ϕ_c was calculated using the following relation:

$$\phi_C = \frac{\Delta H_m}{\Delta H_{m,100}(1-\phi_R)}$$

where ΔH_m is the measured melting enthalpy, $\Delta H_{m,100}$ is the melting enthalpy of 100% crystalline polyamide 6, and ϕ_R is the weight fraction of the reinforcing material [14]. The mobile amorphous phase (MAP) was determined from:

$$\phi_{MAP} = \frac{\Delta C_p}{\Delta C_{p,0}}$$

where ΔC_p is the specific heat increment at the glass transition for the semi-crystalline polymer, and $\Delta C_{p,0}$= 0.48 J/g·K is the specific heat increment for the fully amorphous PLA [14]. The volume fraction of the rigid amorphous phase (RAP), ϕ_{RAP}, was calculated as:

$$\phi_{RAP} = 1 - \phi_{MAP} - \phi_C$$

where ϕ_{MAP} is the volume fraction of the mobile amorphous phase and ϕ_c is the crystalline volume fraction.

XRD analysis was performed using a PANalytical X'Pert Pro MPD diffractometer (Malvern Panalytical, Netherlands) equipped with a Cu K_α radiation source and an X'Celerator detector. The amorphous baseline of the diffractograms was corrected using the asymmetric least squares method. The average crystallite size D_{hkl} was calculated using the Scherrer equation:

$$D_{hkl} \quad (nm) = \frac{K \cdot \lambda}{\beta \cdot \cos\theta} \quad ,$$

where $K = 0.89$ is the shape factor, λ is the X-ray wavelength, β is the full width at half maximum (FWHM) of the peak, and θ is the Bragg angle [32].

Tensile tests were conducted using a Zwick Z20 universal testing machine (ZwickRoell GmbH & Co. KG, Germany). Prior to testing, specimens were conditioned at 25% relative humidity in a desiccator for 4 weeks. Testing was performed at a crosshead speed of 2 mm/min in accordance with EN ISO 527 standard procedures. For each material, five specimens were tested, and the stress–strain curves were averaged point-by-point to obtain representative results. The tensile work was calculated by the numerical integration of the tensile curve.

3. Results and discussion

3.1. Dispersion of the nanoparticles

In heterogeneous materials, neutron scattering occurs at the interfaces between distinct homogeneous phases. In polymer nanocomposites, these interfaces are between the dispersed nanoparticles and the surrounding matrix [33,34]. Consequently, neutron scattering arises at the nanoparticle–matrix interfaces or in the nanoparticle aggregates where matrix infiltration is incomplete. In contrast, interfaces between adjacent nanotubes do not contribute to scattering and are thus not represented in the measured scattering results. Although in the hybrid composites, the carbon fibres and the carbon nanotubes differ in geometry, they are composed of similar carbon-based structures. As a result, they exhibit nearly identical scattering length densities. In contrast, the matrix—composed of macromolecules rich in hydrogen and oxygen—has a significantly lower scattering length density. Therefore, the contrast at both the carbon fibre–matrix and nanotube–matrix interfaces is of similar magnitude, making it challenging to distinguish between their individual contributions to the total scattering intensity.

To isolate the scattering contribution of the nanoparticles, the scattering data of the neat matrix was subtracted from the total scattering of the nanocomposites. Similarly, for hybrid composites, the scattering data of the matrix with carbon fibres alone was subtracted from the hybrid composite data, allowing the visualization of the scattering contribution due exclusively to the nanotubes. This subtraction is only an approximation, because the total coherent small-angle intensity contains both self-terms and cross (interference) terms; subtracting the PLA + CF reference removes the CF and matrix self-terms but leaves the CNT self-term, any CF–CNT cross-terms, and any CNT-induced changes to CF or matrix structure. Only when those cross-terms and structural changes are small compared to the CNT self-term, can the residual be interpreted as a CNT-only signal. In the present study this is a reasonable working approximation because CFs and CNTs are both carbon based (similar neutron scattering length density), so the dominant contrast is between the carbon, and the hydrogen and oxygen containing PLA matrix, making carbon–matrix interfaces the principal scatterers and reducing expected CF–CNT cross-term magnitude [35]. If the dispersion of nanoparticles is improved in hybrid composites (Fig. 1b) compared to nanocomposites (Fig. 1a), a more pronounced increase in scattering intensity should be expected with increasing nanotube content. However, such an enhancement is not clearly observed. One possible explanation may be the presence of nanotube–carbon fibre interfaces, which, like nanotube–nanotube contacts, do not significantly contribute to neutron scattering. These interfaces are not accounted for in the current analytical approach and may obscure the interpretation of dispersion levels based solely on scattering intensity.

To gain deeper insight into the dispersion of nanoparticles within the hybrid composites, the scattering data were further analyzed by fitting the pair distance distribution function, P(r). [36]. As anticipated, increasing the CNT content in the composite results in an increase of the pair distance distribution function, P(r), consistent with the greater number of scattering centers contributing to the scattering signal (Fig. 2a). In composites containing only CNTs, however, the position of the P(r) peak remains unchanged with increasing CNT content. This indicates that the average inter-nanotube distance is not significantly affected by the CNT concentration. Such behavior suggests that the CNTs are dominantly present in aggregated forms, where increasing concentration does not facilitate their improved dispersion at the nanoscale. However, the P(r) profiles of CNT-only composites exhibit an increasingly prominent shoulder with higher CNT loading. This reflects the presence of more elongated scattering objects, implying that although the CNTs remain aggregated, their effective interaction surface with the polymer matrix increases [37,38]. This is likely due to the formation of more extended CNT bundles, which engage with the surrounding matrix over broader areas.

The introduction of CFs in the hybrid composites significantly alters the P(r) behavior (Fig. 2b). A noticeable shift of the P(r) peak toward higher interparticle distances is observed compared to CNT-only systems. This shift indicates that the average spacing between CNTs increases in the presence of CFs, suggesting an improvement in CNT dispersion. Additionally, the P(r) curves for CF-CNT hybrid composites exhibit more elongated and asymmetric shapes than those of the CNT-only composites. This is indicative of more extended nanotube structures and further supports the conclusion that the CNTs are better dispersed within the matrix. At the highest CNT content examined (1 wt % in the hybrid composite), the P(r) peak becomes narrower and bell-

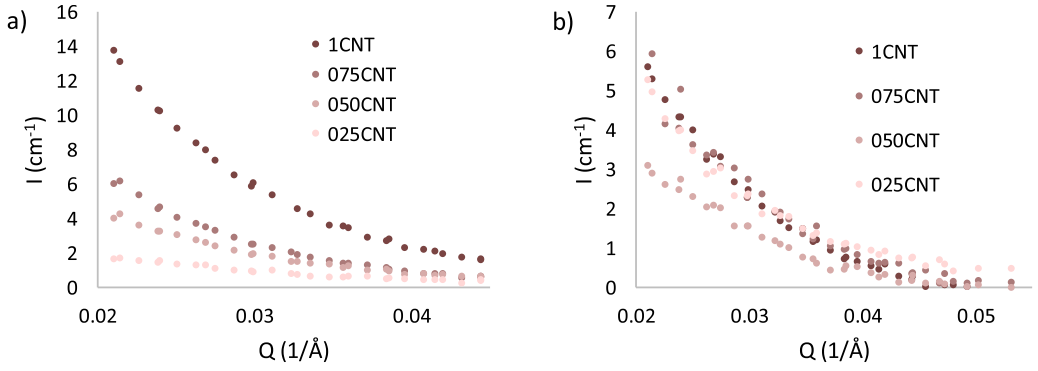

Fig. 1. Small-angle neutron scattering diagrams, a) composites without carbon fibers, b) composites containing 30 wt% carbon fibers.

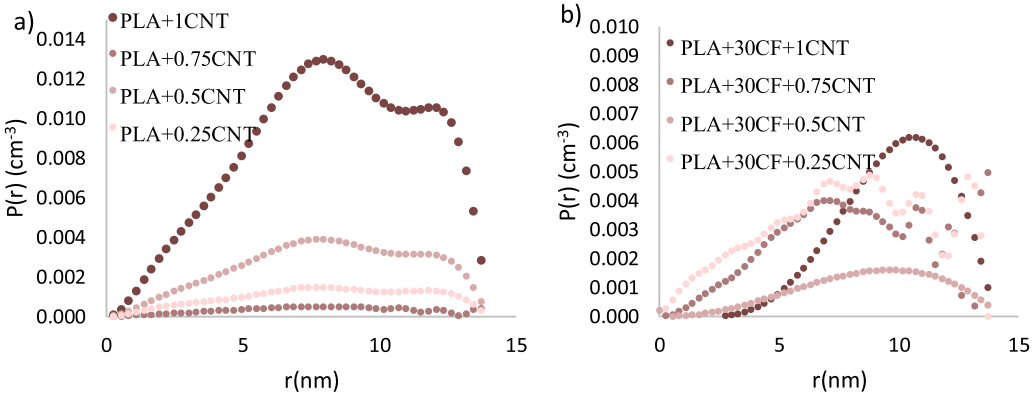

Fig. 2. Pair distance distribution functions calculated from scattering data, a) composites without carbon fibers, b) composites containing 30 wt% carbon fibers.

shaped again, which suggests a decline in dispersion efficiency at this concentration.

The dispersion of the CNTs has a significant impact on the morphology of the matrix material. In post-crystallized PLA matrix composites, three distinct phases can be identified: a crystalline phase, a rigid amorphous phase, and a mobile amorphous phase. Analysis of phase composition reveals that the incorporation of CNTs generally leads to a slight reduction in the crystalline fraction, while increasing the proportion of the rigid amorphous phase compared to neat PLA. One possible explanation for this behavior is that CNTs may act as heterogeneous nucleation sites during crystallization, promoting the formation of a greater number of smaller crystallites. As a result, the surface-to-volume ratio of the crystallites increases, leading to an expanded rigid amorphous interphase surrounding or included in each crystallite. The relationship between CNT content and the relative proportions of each phase is not straightforward, that suggests that local heterogeneities, such as the spatial distribution and size variation of CNT aggregates, significantly influence the crystallization behavior and the resulting phase composition.

3.2. Phase structure of the composites

In the composites containing only nanotubes, increasing the nanotube content slightly increased the crystalline fraction, but did not significantly change the ratio of rigid amorphous to mobile amorphous phases (Fig. 3a). In composites containing only carbon fibres, a reduction in crystallinity is also observed, accompanied by an increase in the rigid amorphous phase (Fig. 3b). This suggests that carbon fibres may promote the formation of smaller crystalline domains, thereby increasing the rigid interfacial region. In hybrid composites containing both carbon fibres and CNTs, a slight further decrease in the crystalline fraction is detected, while the rigid amorphous phase increases substantially (Fig. 3b). This behavior is consistent with the hypothesis in which CNTs serve as nucleation sites in the matrix. Introducing many heterogeneous nucleation sites increases nuclei density but also reduces the space and chain mobility available for crystal growth and creates a rigid amorphous interphase. Under realistic annealing conditions, this leads to many small, impinged and less perfect crystallites and a net reduction of the measured degree of crystallinity. Nucleation is enhanced but growth and lamellar perfection are suppressed, so the total crystalline fraction decreases [39]. However, this trend appears to plateau or even reverse at higher CNT loadings (above 0.75 wt%). At higher concentrations, the increased likelihood of CNT aggregation may reduce effective nucleation density and promote phase overlap, leading to less uniform phase structure.

To investigate the effect of nanoparticles on the crystallization process, DSC measurements were also performed on the non-post-crystallized samples. It can be observed from the DSC curves that the glass transition temperature does not change with increasing nanotube content (Fig. 4). This suggests that nanotubes do not reduce significantly

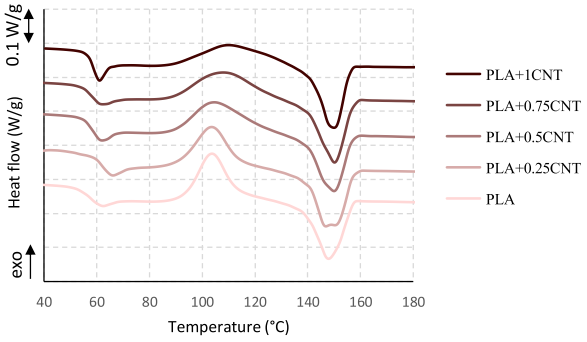

Fig. 4. DSC heating curves of the composites without carbon fibers.

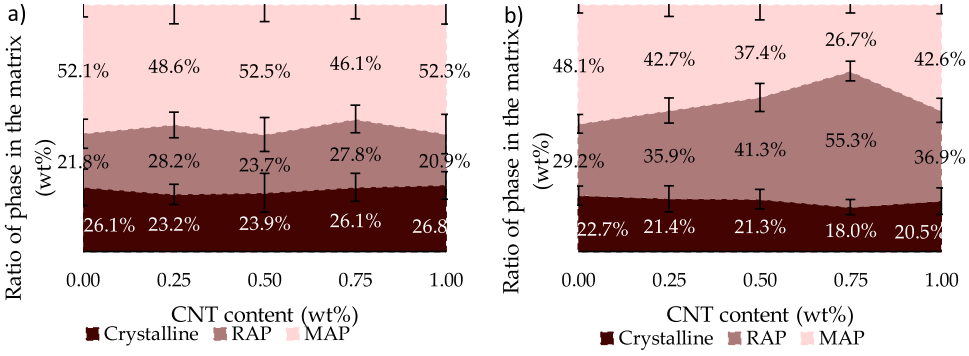

Fig. 3. The ratio of phases forming the matrix of composites, a) composites without carbon fibers, b) composites containing 30 wt% carbon fibers.

the mobility of the molecular chains, not even during cold crystallization. The cold crystallization peak broadens and shifts toward higher temperatures as the CNT concentration increases. This broadening behavior can be attributed to the heterogeneous dispersion of CNTs within the PLA matrix. At low concentrations, CNTs may act as effective heterogeneous nucleating agents, promoting early and relatively uniform crystallization. However, as CNT content increases, dispersion becomes uneven, leading to the remaining of aggregates and regions with varying CNT space filling. This results in spatially non-uniform nucleation behavior: regions with well-dispersed CNTs may crystallize at lower temperatures, while areas with aggregates or insufficient CNTs may exhibit delayed crystallization, thereby contributing to a broadened cold crystallization peak.

In PLA composites containing carbon fibers, the incorporation of CNTs led to a shift of the cold crystallization peak toward lower values (Fig. 5). This observation suggests that both carbon fibers and CNTs act as effective nucleating agents, facilitating earlier onset of crystallization. Furthermore, the cold crystallization peak became sharper and narrower with increasing CNT content. This behavior is indicative of a more uniform and homogeneous dispersion of CNTs within the polymer matrix, which promotes simultaneous crystallization over a shorter time and temperature range due to the spatial uniformity of nucleation sites.

Additionally, the melting endotherm exhibited the emergence of a distinct shoulder at approximately 145 °C. This typically corresponds to a population of less perfect, smaller, or more disordered PLA crystallites. Its appearance further supports the role of uniformly dispersed CNTs in enhancing crystal nucleation, leading to the formation of crystalline domains with a broader size distribution.

3.3. Crystal structure of the composites

XRD studies can reveal the size, shape, and spatial arrangement of crystalline particles more thoroughly, thus allowing a better understanding of their effect on mechanical properties. With increasing CNT content, all diffraction peaks exhibit slightly higher intensity, which is characteristic of enhanced crystallinity within the polymer matrix. Furthermore, a slight narrowing of these peaks is observed, suggesting the growth of larger crystallite domains. These observations support the hypothesis that CNTs act as effective nucleating agents, facilitating the crystallization of PLA and contributing to improved crystal perfection. The carbon nanotube reinforced samples show an increase in peak intensity relative to neat PLA, indicating a nucleating effect of CNTs (Fig. 6a). This is apparent in the significant intensification of the (200)/(110) diffraction peak (α_2). Besides this, other peaks such as (010) and (210) also increase, but to a lesser extent. The preferential intensification of the (200)/(110) planes suggests that CNTs may induce enhanced polymer chain packing, potentially via epitaxial or oriented nucleation mechanisms at the CNT surface. This effect implies an alignment of polymer chains parallel to the CNT axis, which corresponds to the (200)/(110) lattice orientation [40–42]. In samples containing both carbon fibers and CNTs, this behavior is modest, but systematic, the (200)/(110) peak exhibits intensification with CNT loading, while the other peaks shows only modest changes (Fig. 6b). The reason for this may be that in the composite containing only CFs, the CFs themselves already increase the intensity of the (200)/(110) peak, which the addition of carbon nanotubes can only enhance to a lesser extent.

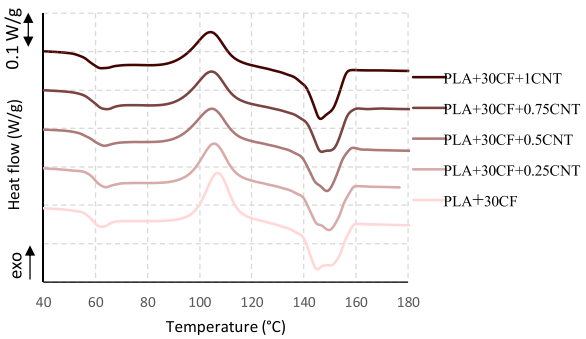

Fig. 5. DSC heating curves of the composites containing 30 wt% carbon fibers.

Crystallite size normal to a given (hkl) plane reflects the dimension of the crystallite perpendicular to that direction—larger values indicate elongation perpendicular to the plane, while smaller values suggest thinner or constrained growth. The $\alpha_1 + \alpha_1'$ plane is oriented normal to the b-axis, representing lateral crystal growth (Fig. 7a) [40–42]. At 30 wt% CF, crystallite sizes reach up to ~50 nm, compared to ~25–35 nm without CF, suggesting enhanced lateral growth. This may result from improved chain packing or fiber-induced orientation during crystallization. The α_2 plane is also indicative of lateral dimensions. These planes exhibit consistently large sizes (40–65 nm) regardless of CF content (Fig. 7b) [40–42]. This points to a lamellar crystalline structure with minimal disruption from reinforcing materials. The $\alpha_3 + \alpha_3'$ plane set also reflects lateral dimensions and exhibits trends similar to $\alpha_1 + \alpha_1'$, with moderate size increases upon CF incorporation, which reinforces the hypothesis of CF-induced lateral ordering (Fig. 7c). The α_4 plane set represents diagonal dimensions across the a and b axes [40–42], crystallite sizes here decrease from ~60 nm (0 wt% CF) to ~35–55 nm (30 wt% CF) (Fig. 7d). This suggests spatial restriction or altered nucleation mechanisms induced by CFs, limiting growth along this mixed-direction plane. The crystal nucleating effect of the reinforcing materials enhances the polymer chains to align along the CF and CNT surface, this promotes planar crystal growth parallel to the fiber, favoring lateral dimensions, as the presence of reinforcement restricts space in specific directions.

This constraint can force crystals to grow outward (laterally) instead of vertically (along the chain axis in PLA), forming a shish-kebab structure around the CNTs (Fig. 8). This results in that when the composite is stressed and the load transfers from the lower modulus matrix to the high modulus fibers, the laterally oriented crystallites between them act as bridges, spreading the stress more effectively across the polymer-fiber boundary. This effect is further increased by the rigid amorphous interphase between (or within) the crystalline parts, and overlapping each other.

3.4. Mechanical properties

In the nano- and hybrid composites, the deformation and failure processes (elastic matrix response, matrix yielding, CNT crack-bridging and pull-out, and fibre-matrix load transfer) are intrinsically multi-stage and overlapping, which usually produce multiple slopes, shoulders and non-monotonic features. The point-by-point averaging of five individual tensile curves on a common strain grid (Fig. 9) smooths these specimen-specific abrupt load drops. This averaging yields a statistically representative, smoother curve that suppresses stochastic specimen and test specific events and therefore facilitates robust comparison of tensile properties and correlation with the microstructural features. In the PLA without CFs, the incremental addition of carbon nanotubes produced no significant change in the elastic modulus or ultimate tensile strength within the experimental scatter, although the PLA + 1CNT specimens exhibited an average tensile strength of 62 MPa compared to the 52 MPa for neat PLA (Fig. 9a). This difference is small relative to sample-to-sample variability, the clearest, reproducible effect of CNTs in the absence of carbon fiber was an increase in elongation at break. By contrast, when 30 wt% carbon fiber was present, CNT incorporation produced a significant improvement in load-bearing performance (Fig. 9b). The CNT-containing hybrid composites show higher tensile strength and larger elongation at break than the CF-only composite, the maximum average tensile strength of 85 MPa can be observed for PLA + 30CF + 1CNT, while the initial modulus decreased slightly. Microstructurally, these enhancements are consistent with more effective CNT dispersion and improved matrix–reinforcement load transfer in

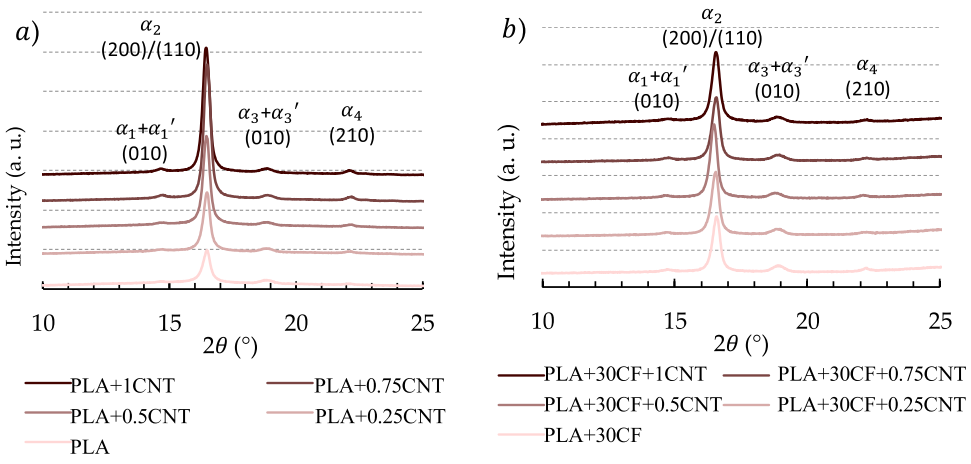

Fig. 6. X-ray diffractograms of a) composites without carbon fibers, b) composites containing 30 wt% carbon fibers.

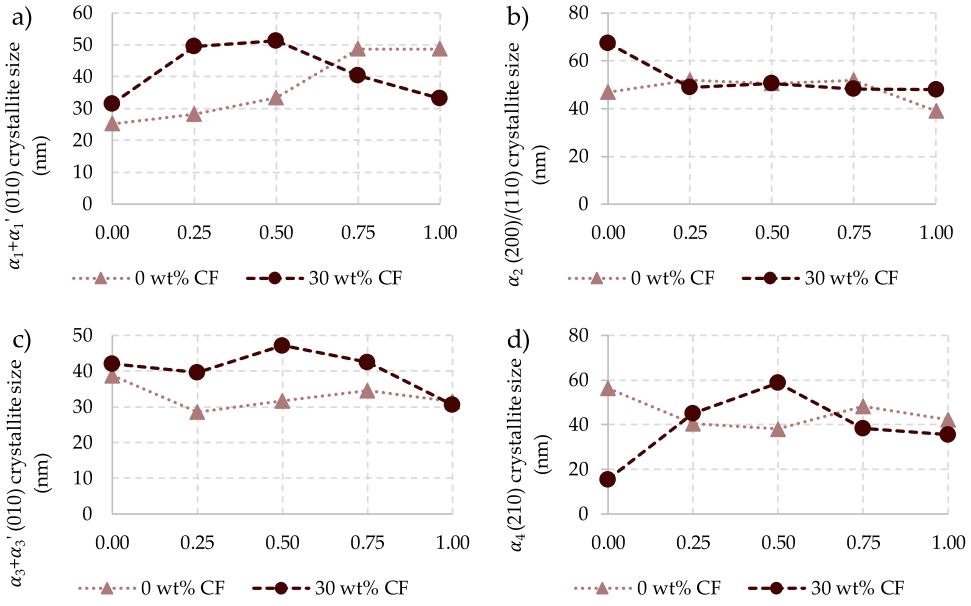

Fig. 7. Crystallite sizes perpendicular to the a) α + α1' planes, b) α2 planes c) α3 + α3' planes, d) α4 planes.

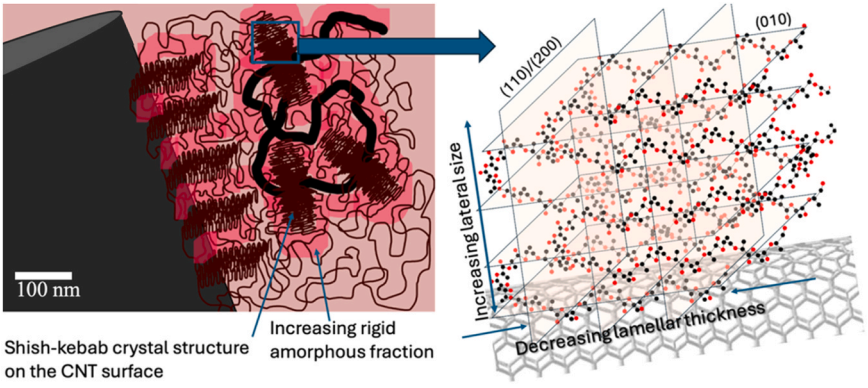

Fig. 8. Phase structure of the carbon fiber and carbon nanotube reinforced hybrid composites.

the hybrid system. The carbon fibers facilitate breakup of CNT aggregates during processing, promoting a more homogeneous nanoparticle distribution and a finer crystalline morphology, both of which facilitate stress transfer, hinder crack growth, and delay failure.

The energy absorption capacity of the composites, quantified as tensile work (Fig. 10), provides additional insight into their toughness behavior. Neat PLA exhibited a tensile work of 0.57 J. Incorporation of 30 wt% CF increased this value to 1.9 J, primarily attributable to the

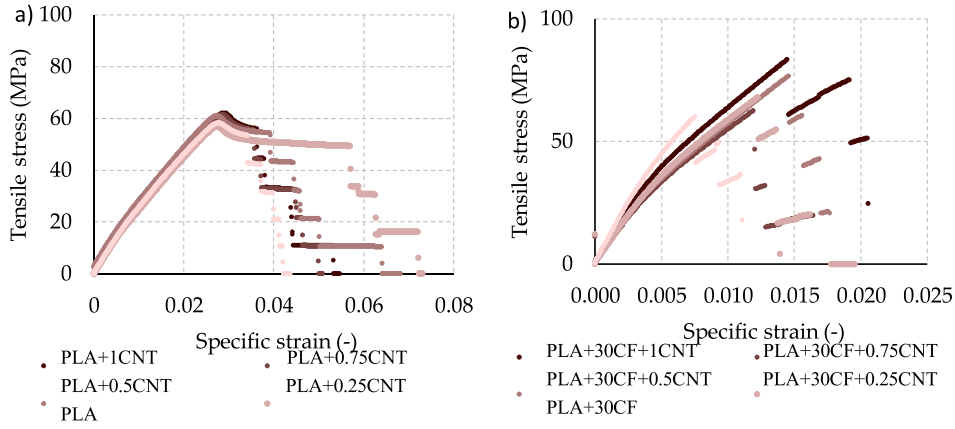

Fig. 9. Averaged tensile curves of the a) composites without carbon fibers, b) composites containing 30 wt% carbon fibers.

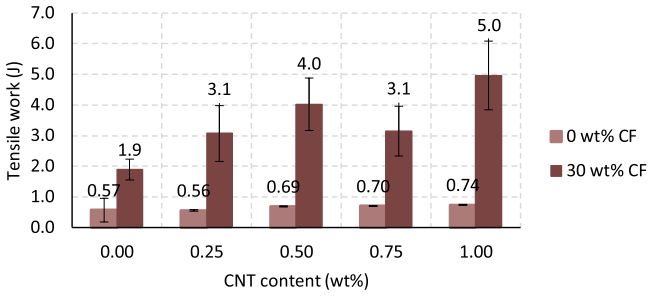

Fig. 10. Tensile work of the composites without carbon fibers and the composites containing 30 wt% carbon fibers.

enhanced modulus and tensile strength, despite the relatively limited elongation at break. The introduction of CNTs further increased the tensile work, predominantly through improvements in elongation at break, while only marginally affecting the modulus. In the PLA + 30 wt % CF system, the addition of CNTs led to a significant enhancement in tensile work, with a maximum value of 5.0 J obtained at 1 wt% CNT. For PLA reinforced only with CNTs, tensile work also exhibited an increasing trend with CNT content, reaching a maximum of 0.74 J at 1 wt% CNT. These findings indicate that while CNT incorporation alone contributes to improved toughness, the combined use of CF and CNTs produces a synergistic effect, resulting in a markedly greater enhancement in energy absorption capacity.

This is explained by that the dispersion state of CNTs dictates whether they act as toughening bridges or stress concentrators, well-dispersed, elongated, matrix-embedded CNT networks bridge cracks, dissipate energy and improve load transfer, increasing toughness and tensile strength, whereas aggregated CNT bundles would nucleate premature failure, lowering tensile strength with little toughness gain. In the hybrid composites, the CFs produce more dispersed CNT network, which explains the large toughness improvements observed. Recent literature shows inconsistent tensile-strength increment for PLA reinforced with either CNTs or short carbon fibers alone. CNT-only systems often reach tensile strength approximately 60–70 MPa and show modest toughness improvements only when CNTs are surface-modified or architected, while short-CF PLA composites frequently increases modulus but not always the tensile strength. Hybrid composites with small CNT content (0.25–1 wt%) can help multifunctionality, but toughness increases are rarely observed without a specific dispersion-assistance mechanism [9,43]. The purely mechanically assisted dispersion of the CNTs by CFs during compounding changes the effective interfacial area, and thus produces a highly effective interphase without the technologically more expensive and complex chemical grafting. The interphase structure formed as a consequence of this, controls local strain transfer by being organized into a shish–kebab crystalline structure, it promotes gradual load transfer and raises toughness and stiffness significantly.

4. Conclusions

To investigate the effect of carbon nanotubes (CNTs) on the morphology and mechanical performance of PLA composites, two material series were produced: nanocomposites with 0–1 wt% CNT and hybrid composites with 30 wt% carbon fiber (CF) and the same CNT concentrations. Small-angle neutron scattering analysis revealed that CNT-only composites showed slight change in inter-nanotube distance, suggesting CNT aggregation. However, the appearance of a shoulder in the pair distance distribution P(r) curves showed the formation of larger, elongated CNT bundles, indicating increased interfacial interactions. The hybrid composites showed a shift in P(r) peak positions, indicating improved CNT dispersion due to the presence of carbon fibers. The asymmetric P(r) profiles in these systems suggest the formation of more extended CNT structures, although dispersion efficiency decreased at 1 wt% CNT due to aggregation. The DSC analysis showed that CNTs and CFs influence PLA crystallization behavior. Both fillers increased the rigid amorphous fraction and reduced overall crystallinity, due to the formation of numerous small crystallites and constrained chain mobility. The hybrid systems exhibited the most pronounced rigid amorphous regions, indicating synergistic nucleation effects, though dispersion declined at higher CNT loadings. X-ray diffraction revealed that reinforcement primarily promoted lateral crystallite growth, indicating a shish-kebab structure around the CNTs. Mechanical tests showed, that CNTs improved both tensile strength and elongation at break, with optimal results observed in hybrid composites. PLA + 30CF + 1CNT achieved the highest tensile strength (85 MPa), improved stiffness, and enhanced load transfer due to better CNT dispersion and refined crystalline morphology. Energy absorption, measured as tensile work, peaked at 2.32 J for PLA + 30CF + 0.25CNT, illustrating the high toughness of hybrid systems. This study demonstrates that short carbon fibers can assist the mechanical dispersion of CNTs in PLA-based hybrid composites, enabling the formation of an effective interphase without the need for chemical modification. The resulting nanostructure facilitates efficient stress transfer and energy dissipation, leading to simultaneous improvements in toughness and stiffness — exceeding the mechanical performance typically achieved with natural fiber reinforcement. While the presence of synthetic fibers reduces the overall biodegradability, the use of a renewable-resource-based PLA matrix still offers significant sustainability benefits. These findings open new pathways for the development of high-performance biocomposites in structural applications where both mechanical reliability and partial environmental compatibility are required.

CRediT authorship contribution statement

Roland Petrény: Writing – original draft, Visualization, Investigation, Conceptualization. **László Almásy:** Writing – review & editing, Investigation. **László Mészáros:** Writing – review & editing, Supervision, Conceptualization.

Declaration of Competing Interest

The authors declare that they have no known competing financial interests or personal relationships that could have appeared to influence the work reported in this paper.

Acknowledgements

The authors acknowledge the Ministry of Culture and Innovation of Hungary for support from the National Research, Development and Innovation Fund through grant no. NKKP ADVANCED 149578.

Data availability

Data will be made available on request.

References

[1] T. Angelin Swetha, V. Ananthi, A. Bora, N. Sengottuvelan, K. Ponnuchamy, G. Muthusamy, A. Arun, A review on biodegradable polylactic acid (PLA) production from fermentative food waste - Its applications and degradation, Int. J. Biol. Macromol. 234 (2023) 123703, https://doi.org/10.1016/j.ijbiomac.2023.123703.

[2] C.S. Reshma, S. Remya, J. Bindu, A review of exploring the synthesis, properties, and diverse applications of poly lactic acid with a focus on food packaging application, Int. J. Biol. Macromol. 283 (2024) 137905, https://doi.org/10.1016/j.ijbiomac.2024.137905.

[3] A. Morão, F. de Bie, Life Cycle Impact Assessment of Polylactic Acid (PLA) Produced from Sugarcane in Thailand, J. Polym. Environ. 27 (2019) 2523–2539, https://doi.org/10.1007/s10924-019-01525-9.

[4] R.A. Ilyas, M.Y.M. Zuhri, H.A. Aisyah, M.R.M. Asyraf, S.A. Hassan, E.S. Zainudin, S. M. Sapuan, S. Sharma, S.P. Bangar, R. Jumaidin, Y. Nawab, A.A.M. Faudzi, H. Abral, M. Asrofi, E. Syafri, N.H. Sari, Natural Fiber-Reinforced Polylactic Acid, Polylactic Acid Blends and Their Composites for Advanced Applications, Polym. (Basel) 14 (2022) 202, https://doi.org/10.3390/polym14010202.

[5] V. Fiore, C. Sanfilippo, L. Calabrese, Dynamic Mechanical Behavior Analysis of Flax/Jute Fiber-Reinforced Composites under Salt-Fog Spray Environment, Polym. (Basel) 12 (2020) 716, https://doi.org/10.3390/polym12030716.

[6] L. Wang, J. Abenojar, M.A. Martínez, C. Santiuste, Degradation of Mechanical Properties of Flax/PLA Composites in Hygrothermal Aging Conditions, Polym. (Basel) 16 (2024) 528, https://doi.org/10.3390/polym16040528.

[7] P. Khalili, X. LIU, Z. ZHAO, B. Blinzler, Fully Biodegradable Composites: Thermal, Flammability, Moisture Absorption and Mechanical Properties of Natural Fibre-Reinforced Composites with Nano-Hydroxyapatite, Mater. (Basel) 12 (2019) 1145, https://doi.org/10.3390/ma12071145.

[8] A. Wang, X. Tang, Y. Zeng, L. Zou, F. Bai, C. Chen, Carbon Fiber-Reinforced PLA Composite for Fused Deposition Modeling 3D Printing, Polym. (Basel) 16 (2024) 2135, https://doi.org/10.3390/polym16152135.

[9] A.A. Ogaili, A. Basem, M.S. Kadhim, Z.T. Al-Sharify, A.A. Jaber, E.K. Njim, L.A. Al-Haddad, M.N. Hamzah, E.S. Al-Ameen, The Effect of Chopped Carbon Fibers on the Mechanical Properties and Fracture Toughness of 3D-Printed PLA Parts: An Experimental and Simulation Study, J. Compos. Sci. 8 (2024) 273, https://doi.org/10.3390/jcs8070273.

[10] A. Selvam, M. Suresh, R. Whenish, R. Velu, B. Subramanian, Preparation and Evaluation of the Tensile Characteristics of Carbon Fiber Rod Reinforced 3D Printed Thermoplastic Composites, J. Compos. Sci. 5 (2020) 8, https://doi.org/10.3390/jcs5010008.

[11] A. da Silva Siqueira, N. Ferreira Braga, P.A. Riveros Muñoz, L. Freitas de Freitas, A. H. Ferreira, G.J.M. Fechine, Biodegradable scaffold: integration of polylactic acid, hydroxyapatite, and graphene oxide via FDM 3D printing, Express Polym. Lett. 18 (2024) 656–672, https://doi.org/10.3144/expresspolymlett.2024.48.

[12] I.D. Posen, P. Jaramillo, W.M. Griffin, Uncertainty in the Life Cycle Greenhouse Gas Emissions from U.S. Production of Three Biobased Polymer Families, Environ. Sci. Technol. 50 (2016) 2846–2858, https://doi.org/10.1021/acs.est.5b05589.

[13] A. Seile, E. Spurina, M. Sinka, Reducing Global Warming Potential Impact of Bio-Based Composites Based of LCA, Fibers 10 (2022) 79, https://doi.org/10.3390/fib10090079.

[14] L. Mészáros, A. Horváth, L.M. Vas, R. Petrény, Investigation of the correlations between the microstructure and the tensile properties multi-scale composites with a polylactic acid matrix, reinforced with carbon nanotubes and carbon fibers, with the use of the fiber bundle cell theory, Compos. Sci. Technol. 242 (2023) 110154, https://doi.org/10.1016/j.compscitech.2023.110154.

[15] Y. Wang, Y. Mei, Q. Wang, W. Wei, F. Huang, Y. Li, J. Li, Z. Zhou, Improved fracture toughness and ductility of PLA composites by incorporating a small amount of surface-modified helical carbon nanotubes, Compos. Part B Eng. 162 (2019) 54–61, https://doi.org/10.1016/j.compositesb.2018.10.060.

[16] J.A. Paz-González, Y. Gochi-Ponce, C. Velasco-Santos, E. Alcudia-Zacarias, A. Zizumbo-López, B. Trujillo-Navarrete, O.A. Morales-Contreras, L.J. Villarreal-Gómez, Enhancing Polylactic Acid/Carbon Fiber-Reinforced Biomedical Composites (PLA/CFRCs) with Multi-Walled Carbon Nanotube (MWCNT) Fillers: A Comparative Study on Reinforcing Techniques, J. Compos. Sci. 9 (2025), https://doi.org/10.3390/jcs9040167.

[17] P. Csvila, T. Czigány, Multifunctional energy storage polymer composites: The role of nanoparticles in the performance of structural supercapacitors, Express Polym. Lett. 18 (2024) 1023–1038, https://doi.org/10.3144/expresspolymlett.2024.78.

[18] K. Kun, A. Bata, F. Ronkay, Investigation of the Replication Quality of Microstructures on Injection Moulded Specimens Made from Recycled Polypropylene Composites Reinforced with Carbon Nanotubes, Period. Polytech. Mech. Eng. 68 (2024) 247–253, https://doi.org/10.3311/PPme.37288.

[19] J. Duan, S. Shao, Ya-Li, L. Wang, P. Jiang, B. Liu, Polylactide/graphite nanosheets/MWCNTs nanocomposites with enhanced mechanical, thermal and electrical properties, Iran. Polym. J. 21 (2012) 109–120, https://doi.org/10.1007/s13726-011-0008-8.

[20] P.A.N. de Yro, K.N.M. Cochon, J.B.P. Rueda, G.M.O. Quiachon, M.L. Ebarvia, B. A. Basilia, PLA/MWCNT Nanocomposite: Improved Electrical, Thermal and Antibacterial Properties for Fused Deposition Modelling Additive Manufacturing Applications, Mater. Sci. Forum 1085 (2023) 29–34, https://doi.org/10.4028/p-04wj70.

[21] C. Zhang, K. Deng, X. Li, K.K. Fu, C. Ni, Thermally Conductive 3D-Printed Carbon-Nanotube-Filled Polymer Nanocomposites for Scalable Thermal Management, ACS Appl. Nano Mater. 6 (2023) 13400–13408, https://doi.org/10.1021/acsanm.3c02067.

[22] R. Petrény, C. Tóth, A. Horváth, L. Mészáros, Development of electrically conductive hybrid composites with a poly(lactic acid) matrix, with enhanced toughness for injection molding, and material extrusion-based additive manufacturing, Heliyon 8 (2022) e10287, https://doi.org/10.1016/j.heliyon.2022.e10287.

[23] J. Luo, H. Wang, D. Zuo, A. Ji, Y. Liu, Research on the Application of MWCNTs/PLA Composite Material in the Manufacturing of Conductive Composite Products in 3D Printing, Micromachines 9 (2018) 635, https://doi.org/10.3390/mi9120635.

[24] F. Weber, V. Dötschel, P. Steinmann, S. Pfaller, M. Ries, Evaluating the impact of filler size and filler content on the stiffness, strength, and toughness of polymer nanocomposites using coarse-grained molecular dynamics, Eng. Fract. Mech. 307 (2024) 110270, https://doi.org/10.1016/j.engfracmech.2024.110270.

[25] N.D. Bikiaris, I. Koumentakou, C. Samiotaki, D. Meimaroglou, D. Varytimidou, A. Karatza, Z. Kalantzis, M. Roussou, R.D. Bikiaris, G.Z. Papageorgiou, Recent Advances in the Investigation of Poly(lactic acid) (PLA) Nanocomposites: Incorporation of Various Nanofillers and their Properties and Applications, Polym. (Basel) 15 (2023) 1196, https://doi.org/10.3390/polym15051196.

[26] A.R. Liu, B.Z. Xu, C.C. Chen, D.Y. Huang, E.W. Liang, F.X. Ge, G.J. Ge, Effects of modified SWCNT on the mechanical and thermal properties of PLA/PHB bio-composites, AIP Adv. 10 (2020) 75122, https://doi.org/10.1063/5.0011522.

[27] H.S. Patanwala, D. Hong, S.R. Vora, B. Bognet, A.W.K. Ma, The microstructure and mechanical properties of 3D printed carbon nanotube-polylactic acid composites, Polym. Compos 39 (2018) E1060–E1071, https://doi.org/10.1002/pc.24494.

[28] J. Sharifi, G. Rizvi, H. Fayazfar, Toward Sustainable 3D-Printed Sensor: Green Fabrication of CNT-Enhanced PLA Nanocomposite via Solution Casting, Mater. (Basel) 17 (2024) 5782, https://doi.org/10.3390/ma17235782.

[29] F. De Santis, V. Volpe, R. Pantani, Effect of molding conditions on crystallization kinetics and mechanical properties of poly(lactic acid), Polym. Eng. Sci. 57 (2017) 306–311, https://doi.org/10.1002/pen.24414.

[30] L. Rosta, Cold neutron research facility at the Budapest Neutron Centre, Appl. Phys. A. 74 (2002) s52–s54, https://doi.org/10.1007/s003390201387.

[31] L. Almásy, New Measurement Control Software on the Yellow Submarine SANS Instrument at the Budapest Neutron Centre, J. Surf. Investig. X-Ray Synchrotron Neutron Tech. 15 (2021) 527–531, https://doi.org/10.1134/S1027451021030046.

[32] J.R.H. Ross, in: J.R.H.B.T.-C.C. Ross (Ed.), Chapter 5 - Catalyst Characterization, Elsevier, Amsterdam, 2019, pp. 121–132, https://doi.org/10.1016/B978-0-444-63474-0.00005-9.

[33] O. Holderer, A.-C. Genix, M. Kruteva, J. Oberdisse, Editorial: Nanocomposites with interfaces controlled by grafted or adsorbed polymers, Front. Phys. 10 (2023) 1117549, https://doi.org/10.3389/fphy.2022.1117549.

[34] R. Petrény, L. Almásy, L. Mészáros, Investigation of the interphase structure in polyamide 6–matrix, multi-scale composites, Compos. Sci. Technol. 225 (2022) 109489, https://doi.org/10.1016/j.compscitech.2022.109489.

[35] A. Guinier, G. Fournet, Small-angle Scattering of X-rays, Wiley, 1955. ⟨https://books.google.hu/books?id=TMLQAAAAMAAJ⟩.

[36] P.F. Peterson, D. Olds, M.T. McDonnell, K. Page, Illustrated formalisms for total scattering data: a guide for new practitioners, J. Appl. Crystallogr 54 (2021) 317–332, https://doi.org/10.1107/S1600576720015630.

[37] D. Lombardo, P. Calandra, M.A. Kiselev, Structural Characterization of Biomaterials by Means of Small Angle X-rays and Neutron Scattering (SAXS and SANS), and Light Scattering Experiments, Molecules 25 (2020) 5624, https://doi.org/10.3390/molecules25235624.

[38] K. Nishi, M. Shibayama, 2D pair distribution function analysis of anisotropic small-angle scattering patterns from elongated nano-composite hydrogels, Soft Matter 13 (2017) 3076–3083, https://doi.org/10.1039/C6SM02350A.
[39] K. Majerczak, D. Wadkin-Snaith, V. Magueijo, P. Mulheran, J. Liggat, K. Johnston, Polyhydroxybutyrate: a review of experimental and simulation studies of the effect of fillers on crystallinity and mechanical properties, Polym. Int. 71 (2022) 1398–1408, https://doi.org/10.1002/pi.6402.
[40] K. Wasanasuk, K. Tashiro, M. Hanesaka, T. Ohhara, K. Kurihara, R. Kuroki, T. Tamada, T. Ozeki, T. Kanamoto, Crystal Structure Analysis of Poly(l-lactic Acid) α Form On the basis of the 2-Dimensional Wide-Angle Synchrotron X-ray and Neutron Diffraction Measurements, Macromolecules 44 (2011) 6441–6452, https://doi.org/10.1021/ma2006624.
[41] A. Farahani, A. Zarei-Hanzaki, H.R. Abedi, L. Tayebi, E. Mostafavi, Polylactic Acid Piezo-Biopolymers: Chemistry, Structural Evolution, Fabrication Methods, and Tissue Engineering Applications, J. Funct. Biomater. 12 (2021) 71, https://doi.org/10.3390/jfb12040071.
[42] S. Lee, M. Kimoto, M. Tanaka, H. Tsuji, T. Nishino, Crystal modulus of poly (lactic acid)s, and their stereocomplex, Polym. (Guildf.) 138 (2018) 124–131, https://doi.org/10.1016/j.polymer.2018.01.051.
[43] M.M. Younus, H.M. Naguib, M. Fekry, M.A. Elsawy, Pushing the limits of PLA by exploring the power of MWCNTs in enhancing thermal, mechanical properties, and weathering resistance, Sci. Rep. 13 (2023) 16588, https://doi.org/10.1038/s41598-023-43660-3.